Shear-Induced Configurations of Confined Colloidal Suspensions

Itai Cohen,[1] Thomas G. Mason,[2] and David A. Weitz[1]

[1]*Department of Physics and Division of Engineering and Applied Sciences, Harvard University, 9 Oxford Street, Cambridge, Massachusetts 02138, USA*

[2]*Department of Chemistry and Biochemistry and Department of Physics and Astronomy, University of California at Los Angeles, 607 Charles E. Young Drive, Los Angeles, California 90095, USA*

(Received 10 January 2004; published 23 July 2004)

We show that geometric confinement dramatically affects the shear-induced configurations of dense monodisperse colloidal suspensions; a new structure emerges, where layers of particles buckle to stack in a more efficient packing. The volume fraction in the shear zone is controlled by a balance between the viscous stresses and the osmotic pressure of a contacting reservoir of unsheared particles. We present a model that accounts for our observations and helps elucidate the complex interplay between particle packing and shear stress for confined suspensions.

DOI: 10.1103/PhysRevLett.93.046001 PACS numbers: 83.10.Tv, 47.54.+r, 82.70.Dd, 83.85.Ei

Colloidal suspensions in thermodynamic equilibrium exhibit fascinating phase behavior, controlled by a delicate interplay between interparticle interactions and volume exclusion. Packing constraints are essential for determining the structures that result and an understanding of these has been instrumental in elucidating the phase behavior formed by colloidal suspensions under various conditions. These include the packing of spherical particles in bulk [1,2] and the unavoidable defects formed when particles order on the surface of a spherical drop [3]. Exposing such suspensions to large strains can drive them out of equilibrium and significantly modify the particle configurations; nevertheless, the shear stresses can still effectively thermalize the particles, allowing them to explore their phase space and adopt reproducible structures. For example, in bulk, a dense suspension of monodisperse particles subjected to oscillatory shear will order into hexagonally close-packed (hcp) layers oriented parallel to the shearing plates [4–7]. The shear-induced viscous stresses force adjacent layers to separate allowing them to flow over one another, and the particle velocity and the amplitude of the motion vary linearly between the shearing plates [4–7]. While these structures have been well described, the complex interplay between particle packing and the shear induced stresses which leads to formation of these structures is still poorly understood.

When a dense suspension of monodisperse particles is geometrically confined between two plates but not subjected to shear, the packing constraints force the suspension to adopt equilibrium structures different from those observed in bulk [8–11]. Subjecting such highly confined suspensions to shear is of considerable technological relevance to coatings, lubricants, and biorheology [12–14]; moreover, the limited number of particle layers may facilitate a more quantitative analysis of the stresses, and a direct determination of the interplay between packing and shear-induced stresses, allowing the resultant nonequilibrium structures to be explicitly determined. Surprisingly, such highly confined suspensions subjected to shear have never been investigated.

In this Letter, we investigate dense colloidal suspensions highly confined between two flat plates and subjected to large oscillatory shear. We show that confinement forces the suspension to adopt structures that are translationally invariant along the direction of particle motion and include striking gaps in the packing which, nevertheless, allow the particles to pack more efficiently than those observed in bulk. We present a model that accounts for our observations by elucidating the interplay between shear stress, particle packing, and geometric confinement that leads to these ordered, but highly nonequilibrium structures.

The suspensions contain spherical poly-(methylmethacrylate) (PMMA) particles sterically stabilized by a thin layer of poly-12-hydroxystearic acid [15–17]. The particles are impregnated with rhodamine dye and suspended in a mixture of cyclohexyl bromide, tetralin, and decalin, chosen to match both the index of refraction and density of the particles. This procedure allows us to view the three dimensional structure of the suspension using fluorescence and confocal microscopy [16]. Optical tweezers measurements [18] and electrophoretic mobility measurements show that the dying process imparts a positive charge onto the particles. The liquid-crystal coexistence regime for these particles is shifted and has been shown to occur at a particle volume fraction $0.38 < \phi < 0.42$ [19], whereas in hard spheres, this regime occurs at $0.494 < \phi < 0.545$. While the experiments described in this Letter use charged particles, preliminary experiments using particles that are significantly less charged reproduce the observed phenomena and indicate that charging effects play a secondary role in the observed pattern formation. The solvent mixture viscosity $\eta_0 = 0.023$ P. The particles have a diameter $d = 1.42$ μm and polydispersity of 5%.

Our apparatus [20] mounts on an inverted microscope and allows 3D visualization of a suspension with control

over gap separation, shear frequency, and shear amplitude. The suspension is sheared between a fixed plate 5 mm in diameter and a movable microscope coverslip, both of which are flat on the particle length scale. Set screws fix the gap, D, between 1 and 100 μm, and align the plates so they are parallel to within 1 μm over the shear zone. A sinusoidally driven piezoelectric actuator moves the coverslip and produces up to 30 μm displacements at frequencies, f, ranging between 0 and 100 Hz. The 5 mm plate is immersed in the suspension so particles in the shear zone contact a large reservoir of particles fixed at volume fraction, $\phi = 0.61 \pm 0.02$. The cell is enclosed so no solvent evaporates. This lets us work with the suspensions for periods longer than a year.

To drive the suspension out of equilibrium, we shear with maximum strains, $\gamma \gtrsim 0.3$ and frequencies, $f \gtrsim 5$ Hz. A phase diagram of the transition from equilibrium to nonequilibrium structures as a function of γ and f will be shown elsewhere [21]. When the gap holds more than 11 layers, the morphology is identical to that in bulk suspensions [Fig. 1(a)]. However, when the gap holds fewer than 11 layers, confinement plays a critical role. The hcp layer structure becomes intermittent, occurring only at discrete plate separations. For gaps incommensurate with these separations, we observe a remarkable new ordering [Figs. 1(b)–1(e)]. Fluid voids appear within the planes and the layers break up into hcp strips aligned in the direction of plate motion, x. Moreover, the strip widths vary with depth, z. A typical example obtained for a gap slightly smaller than that confining four flat layers is shown by the series of x-y images in Figs. 1(b)–1(e). Near the stationary upper plate, the strips are three particles wide and have fluid voids between them [Fig. 1(b)]. In a plane 1.3 μm lower, particles orient in two-particle-wide strips, alternating with one-particle-wide strips [Fig. 1(c)]. Remarkably, the velocity of the two-particle-wide strips is larger than that of the one-particle-wide strips. This structure repeats 1.3 μm farther down, but this time the velocity of the one-particle-wide strips is larger [Fig. 1(d)]. Finally, 1.3 μm farther down, the layer nearest the bottom shearing plate is again oriented into three-particle-wide strips separated by fluid voids [Fig. 1(e)]. It is convenient to examine the strips along the hcp lattice vector directions. Inspection of Fig. 1(b) along the y' axis shows that the three-particle-wide strips are registered. Microscopy measurements indicate the registration arises from interdigitation with the one-particle-wide strips which align with the fluid voids but are located in the plane 1.3 μm below [Fig. 1(c)]. This configuration forces the one- and three-particle-wide strips to have equal velocities. Similar interdigitation is observed for the two-particle-wide strips in Figs. 1(c) and 1(d). Again, the interdigitation forces the strips in different layers to have equal velocities. Finally, similar behavior is observed for the one- and three-particle-wide strips in Figs. 1(d) and 1(e).

We summarize this behavior in the y'-z schematic of the particle positions shown in Fig. 2. The dashed lines indicate the z position of the x-y planes depicted in Figs. 1(b)–1(e). The shadings delineate particles in contact and moving with equal velocities. This figure shows the peculiar patterns result from a buckling of the colloidal and lubricating fluid layers. The particle velocity and oscillation amplitude of the buckled particle layers still vary linearly between the shearing plates. Since the two sets of particle strips shown in Figs. 1(c) and 1(d) belong to different layers they move with different velocities. This is in sharp contrast with the behavior of sheared bulk suspensions where the layers always remain flat.

In confined unsheared suspensions, the reservoir osmotic pressure, Π_{res}, sets the volume fraction of particles in the gap. Then, the interplay between the particle osmotic pressure in the gap and the confined geometry determines the suspension structure [8,9]. When the shear rate is large enough to produce nonequilibrium structures, the viscous stress, τ_η, dominates and determines the suspension structure. Therefore, the effective pressure arising from the shear stress [22] must balance Π_{res} to determine the volume fraction in the shear zone. If we start with a commensurate configuration and increase the

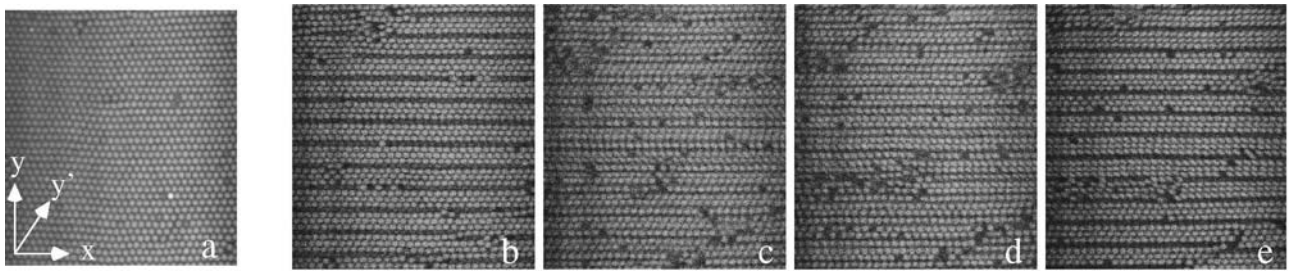

FIG. 1. Structure of a sheared suspension with $\gamma = 0.38$, $f = 30$ Hz, and $\phi = 0.61$. The plate moves in the x direction. (a) shows a confocal micrograph of a sheared suspension forming hcp layers when $D = 80$ μm. (b)–(e) show micrographs of the suspension in the buckled state. The gap is set slightly below the height commensurate with confinement of four flat hcp layers. (b) shows an x-y image slice of the suspension near the upper plate. (c)–(e) show slices that are, respectively, 1.3, 2.6, and 3.9 μm below the slice in (b). The images are presented side by side so that the strip alignment can be compared. The y' direction is aligned with one of the characteristic hcp lattice vectors and forms a 60° angle with the x direction. The x, y, and y' directions are indicated in the bottom left corner of (a).

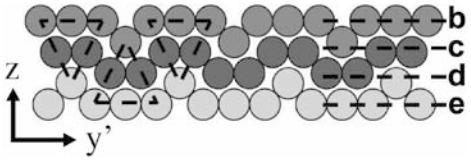

FIG. 2. Suspension structure in the y'-z plane.

gap keeping the layers flat, τ_η will decrease since there will be more fluid between the layers. To maintain the balance between τ_η and Π_{res} the layers must increase their volume fraction. However, due to the constraints imposed by the confined geometry, sufficiently dense packing cannot be achieved with flat hcp layers. Instead, the system must adopt a buckled configuration. The shear stress forces the suspension to have translational invariance along the direction of particle motion. Thus the suspension cannot adopt a configuration which corresponds to an optimized 3D packing. Instead, it must optimize its packing within the y'-z plane. Indeed, eliminating the fluid gaps and grouping the particles into triangles (Fig. 2), we find the buckled structures resemble the densest 2D packing of static hard disks under incommensurate confinement [23].

To estimate τ_η, we consider a gap where the suspension forms flat hcp layers. Since the shear takes place in the lubricating fluid between the layers, the effective viscosity, η_{eff}, of the combined structure is $\eta_{\text{eff}} = \eta_0 D/\sum_i l_i$, where l_i is the thickness of the ith lubricating fluid layer. The viscous stress is $\tau_\eta \approx \gamma f \eta_{\text{eff}}$. Intriguingly, the hcp layer structure introduces an ambiguity in the calculation since different flow configurations lead to different l_i. Nevertheless, we can calculate τ_η for two limiting flow configurations. In the straight flow configuration, particles move directly over the peaks of the hcp sheet below. In this case, we set $l_i = 0$ when the peaks touch and the interlayer distance is d. In the zigzag flow configuration, particles move above the valleys formed by particles in the layer below [5]. In this case, we set $l_i = 0$ when the interlayer distance is $d\sqrt{3}/2$. This is the minimum separation for flow configurations constrained to move without transverse displacements. By measuring the interlayer spacing for the different flows, we find that $\tau_\eta \approx 6.0$ dyn/cm^2 independent of the flow configuration. This stress must balance Π_{res} to ensure no net flux of particles between the shear zone and the reservoir. Simulations of unsheared disordered hard spheres [24] show $\Pi = 1.1$ dyn/cm^2 when $\phi = 0.61$. Furthermore, in charged spheres Π can easily reach 6 times this value [25]. Thus, the stress balance is consistent with our observations.

This stress balance helps determine the nonequilibrium structure of the suspension for small D. We define $\tilde{D} \equiv D/d$, set $\gamma f = 30$ s^{-1}, and, in Fig. 3, plot τ_η versus $\tilde{D}$ for structures with up to ten layers. The solid and dashed curves correspond to τ_η values calculated for straight and zigzag flow configurations, respectively. The horizontal

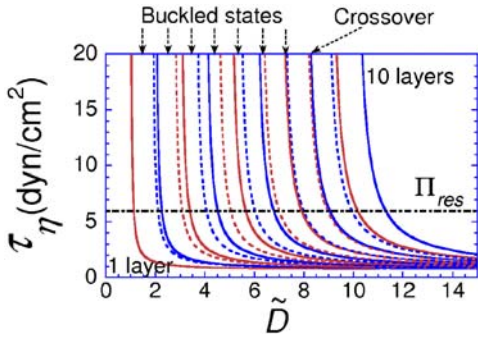

FIG. 3 (color online). Transition mechanism predicting buckling in confined suspensions. The solid and dashed curves indicate τ_η versus the rescaled gap, $\tilde{D}$, for systems with up to ten layers. The solid curves correspond to flat hcp sheets moving in the straight flow configuration. The dashed curves correspond to the zigzag flow configurations and delineate the border between the zigzag and buckled phases. With increasing gap, the buckled region becomes smaller and eventually disappears when the dashed and solid curves cross. The horizontal dash-dotted line corresponds to the value of Π_{res}.

dash-dotted line denotes $\Pi_{\text{res}} = 6.0$ dyn/cm^2. At each gap, the system must assume a structure where $\tau_\eta = \Pi_{\text{res}}$. Therefore, as $\tilde{D}$ is reduced, a system initially in a straight flow configuration must increase the amount of zigzag with which the flat hcp layers move. For systems with fewer than eight layers, the stress curves for such configurations always reside between a solid curve at high $\tilde{D}$ and a dashed curve at low $\tilde{D}$ (Fig. 3). However, as $\tilde{D}$ is reduced further, the system must form a buckled structure with one fewer layer. Further reduction in $\tilde{D}$ causes the amplitude of the buckles to decrease. Eventually the layers become flat and the system is described by the next solid stress curve with one fewer flat layers.

We can further confirm this picture by accounting for the disappearance of the buckled state at large gaps. The $\tilde{D}$ separation between the dashed curves in Fig. 3 is smaller than that of the solid curves. Consequently, the buckled state regions shrink with increasing $\tilde{D}$ and eventually vanish when the curves cross. The curve crossing indicates that more than one flow configuration satisfies the pressure balance for gaps with more than eight layers. To investigate this crossover in the experiments, we fix $\gamma f = 30$ s^{-1} and plot the separation between the top and bottom layers, $\Delta\tilde{D}_{tb}$, for the maximally buckled (open symbols) and straight (closed symbols) flow configurations with different numbers of layers (Fig. 4). This measurement indicates the crossover appears when the system reaches 12 layers. The mismatch in crossover values suggests that in the straight flow configuration, the hcp sheets also move with some degree of registration so that the minimum interlayer separation is less than d. Indeed, even in the buckled state, where layers move with the least amount of zigzag, ping-pong-ball models show the minimum interlayer separation is $0.94d$. This separation would lead to a crossover at 13 flat layers, which is in excellent accord with our observations.

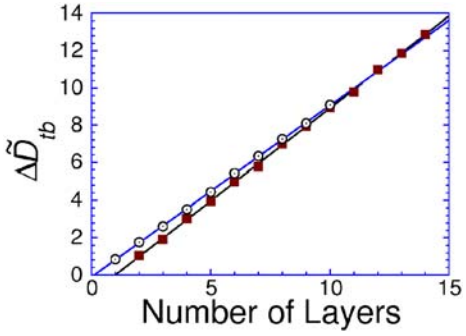

FIG. 4 (color online). Separation between the top and bottom layers, $\Delta\tilde{D}_{tb}$, for maximally buckled (open symbols) and straight (closed symbols) flow configurations with different numbers of layers. The measurement error is on the order of the symbol size. The shear rate $\gamma f = 30\ \mathrm{s}^{-1}$. A crossover of the curves occurs when the layer number is 12.

An additional test of the model is obtained by observing how the slope of the linear fit to the buckled state data in Fig. 4 changes with shear rate. By varying γf, the position where the dashed τ_η curves intersect the Π_{res} line shifts. Therefore, the manner in which the $\tilde{D}$ spacing between the τ_η curves varies predicts the shear rate dependence of the slope. For $0.3 < \gamma f < 30\ \mathrm{s}^{-1}$, the range of shear rates over which the measurements could be taken; the predicted slope is 0.95 at $\gamma f = 30\ \mathrm{s}^{-1}$ and slowly approaches $0.87(\approx \sqrt{3}/2)$ as the shear rate is reduced. In the experiments, we observe a slope of 0.92 ± 0.05 at $\gamma f = 30\ \mathrm{s}^{-1}$, which gradually decreases to 0.89 ± 0.05 at $\gamma f = 0.3\ \mathrm{s}^{-1}$. Again, the measurements are in excellent agreement with the predictions.

Our experiments clearly elucidate the complex interplay between the reservoir osmotic pressure and the shear stress in determining the unusual packings of confined colloidal suspensions subjected to high shear. Our results represent an important instance in which the nonequilibrium configurations of a sheared suspension can be determined. Similar effects will occur and must be considered in other flow geometries provided the shear stress dominates in the shear zone and the osmotic pressure dominates in the reservoir; for example, such an interplay would be expected in a standard rheometer with a Couette geometry. This interplay may allow for tuning of the sheared suspension's rheological properties. Finally, since the observed structures are a consequence of sphere packing in confined geometries, such packing considerations may also impact the trends observed in the shear of very thin atomic and granular films [26–28].

We thank Jacob Israelachvili, Sidney Nagel, Bruce Ackerson, David Leighton, John Brady, and Darren Link for helpful discussions and Andrew Schofield and Peter Pusey for the PMMA particles. Finally, we gratefully acknowledge the financial support of the NSF DMR-0243715, and NASA NAG3-2284 and NAG3-2381 grants.

[1] S. M. Ilett, A. Orrock, W. C. K. Poon, and P. N. Pusey, Phys. Rev. E **51**, 1344 (1995).
[2] A. Yethiraj and A. van Blaaderen, Nature (London) **421**, 513 (2003).
[3] A. R. Bausch, M. J. Bowick, A. Cacciuto, A. D. Dinsmore, M. F. Hsu, D. R. Nelson, M. G. Nikolaides, A. Travesset, and D. A. Weitz, Science **299**, 1716 (2003).
[4] N. A. Clark, A. J. Hurd, and B. J. Ackerson, Nature (London) **281**, 57 (1979).
[5] B. J. Ackerson, J. Rheol. (N.Y.) **34**, 553 (1990).
[6] C. Dux, H. Versmold, V. Reus, T. Zemb, and P. Lindner, J. Chem. Phys. **104**, 6369 (1996).
[7] M. D. Haw, W. C. K. Poon, and P. N. Pusey, Phys. Rev. E **57**, 6859 (1998).
[8] P. Pieranski, L. Strzelecki, and B. Pansu, Phys. Rev. Lett. **50**, 900 (1983).
[9] D. H. Van Winkle and C. A. Murray, Phys. Rev. A **34**, 562 (1986).
[10] J. A. Weiss, D. W. Oxtoby, D. G. Grier, and C. A. Murray, J. Chem. Phys. **103**, 1180 (1995).
[11] S. Neser, C. Bechinger, P. Leiderer, and T. Palberg, Phys. Rev. Lett. **79**, 2348 (1997).
[12] *Proceedings of the Fourth International Congress on Rheology*, edited by A. L. Copley (John Wiley & Sons, Inc., New York, 1963).
[13] D. J. Shaw, *Introduction to Colloid and Surface Chemistry* (Butterworths, Boston, London, 1980).
[14] J. N. Israelachvili, *Intermolecular and Surface Forces* (Academic Press, San Diego, London, 1991).
[15] E. R. Weeks, J. C. Crocker, A. C. Levitt, A. Schofield, and D. A. Weitz, Science **287**, 627 (2000).
[16] A. D. Dinsmore, E. R. Weeks, V. Prasad, A. C. Levitt, and D. A. Weitz, Appl. Opt. **40**, 4152 (2001).
[17] L. Antl, J. W. Goodwin, R. H. Ottewill, S. M. Owens, S. Papworth, and J. A. Waters, Colloids Surf. **17**, 67 (1986).
[18] J. C. Crocker, J. A. Matteo, A. D. Dinsmore, and A. G. Yodh, Phys. Rev. Lett. **82**, 4352 (1999).
[19] U. Gasser, E. R. Weeks, A. Schofield, P. N. Pusey, and D. A. Weitz, Science **292**, 258 (2001).
[20] I. Cohen, T. G. Mason, G. Carver, D. A. Weitz, and J. N. Israelachvili (to be published).
[21] I. Cohen and D. A. Weitz (to be published).
[22] P. R. Nott and J. F. Brady, J. Fluid Mech. **275**, 157 (1994).
[23] P. Pieranski and J. Finney, Acta Crystallogr. Sect. A **35**, 194 (1979).
[24] L. V. Woodcock, Ann. N.Y. Acad. Sci. **371**, 274 (1981).
[25] S. Phan, W. B. Russel, Z. Cheng, J. Zhu, P. M. Chaikin, J. H. Dunsmuir, and R. H. Ottewill, Phys. Rev. E **54**, 6633 (1996).
[26] J. N. Israelachvili, P. M. McGuiggan, and A. M. Homola, Science **240**, 189 (1988).
[27] J. P. Gao, W. D. Luedtke, and U. Landman, Phys. Rev. Lett. **79**, 705 (1997).
[28] D. M. Mueth, G. F. Debregeas, G. S. Karczmar, P. J. Eng, S. R. Nagel, and H. M. Jaeger, Nature (London) **406**, 385 (2000).